Giuseppe Colafemmina; Gerardo Palazzo; Helena Mateos; Samiul Amin; Anne-Laure Fameau; Ulf Olsson; Luigi Gentile*

The cooling process effect on the bilayer phase state of the CTAC/cetearyl alcohol/water surfactant gel,

Colloids and Surfaces A: Physicochemical and Engineering Aspects,

Volume 597,

2020,

Pages 124821,

https://doi.org/10.1016/j.colsurfa.2020.124821.

(https://www.sciencedirect.com/science/article/abs/pii/S0927775720304143)

The cooling process effect on the bilayer phase state of the CTAC/cetearyl alcohol/water surfactant gel

Giuseppe Colafemmina[1], Gerardo Palazzo[1], Helena Mateos[1], Samiul Amin[2], Anne-Laure Fameau[3], Ulf Olsson[4], Luigi Gentile[1*]*

[1] *Department of Chemistry, University of Bari, and CSGI (Center for Colloid and Surface Science), via Orabona 4, 70125, Bari, Italy*

[2] *Department of Chemical Engineering, Manhattan College, New York, USA.*

[3] *L'ORÉAL Recherche & Innovation, Saint-Ouen, France.*

[4]*Division of Physical Chemistry, Lund University, Lund, Sweden.*

Abstract

Gel formation by surfactant molecules is generally controlled by thermodynamics rather than kinetics. Mixtures of long-chain alcohols and surfactants are widely used in various cosmetic and pharmaceutical products. The cooling rate used to produce the products is known to be a key parameter to control the rheological properties and the final texture. However, the physical-chemistry links between the cooling process and the rheological properties are still unknown. Here, we investigated the mechanical properties and microstructure of a surfactant gel formulated with cetyltrimethylammonium chloride (CTAC) and cetearyl alcohol in water by using a multi-technique approach involving rheology, small-angle X-ray scattering (SAXS) and diffusion NMR. The gels, formed by two cooling processes fast and slow cooling, respectively from a high-temperature mixture, have locally a lamellar structure with periodic repeat distances of 31.4 and 28.5 nm for fast and slow cooling, respectively. The cross-polarized microscopy images reveal the presence of multilamellar vesicles (MLVs). These data on the supramolecular aggregates allow rationalizing the mechanical behavior of the two samples. In fact, the elastic, G′, and the viscous, G″, moduli were detected to be ca. 4 times higher for the fast-cooling (quenched) sample than for the slow-cooling (relaxed) sample.

From a fundamental point of view, this study shows that the cooling process is a key parameter in fatty alcohol/surfactant mixture governing the ratio between the bilayer phase states of the two components. From an applied point of view, this finding highlights the key

role of the cooling process on the rheological properties of cosmetic products based on fatty alcohol due to changes happening at the bilayer scale.

1. Introduction

Long-chain fatty alcohols are amphiphilic molecules commonly associated with surfactants in aqueous solution to produce cosmetic and pharmaceutical cream products. The long-chain fatty alcohol is usually a homologous admixture of cetyl and stearyl alcohols with 16 and 18 carbon atoms in the alkyl chain, respectively. Long-chain fatty alcohols, such as stearyl alcohols, are generally combined with long-chain quaternary ammonium surfactants such as cetyltrimethylammonium chloride (CTAC) in formulations of conditioners. [1–3]. The cationic surfactant concentration in conditioners is generally of the order of 1–2% and the alcohols concentrations are usually equal to or greater than those of the cationic surfactants. At appropriate concentrations, the association of these two components leads to the formation of lamellar gel networks at the origin of the creamy texture. [2,4,5] Lamellar gel (also called "α-gel") is a multi-phase colloidal structure mainly composed of lamellar L_β phase, bulk water and (when present in the formulation) oil droplets. The lamellae of the L_β phase are bilayers made of a hexagonally packed crystal of surfactants and fatty alcohols below their melting points spaced by inter-lamellar aqueous layers. [4,6,7] Distinctive of the α-gel structure is a sharp peak in the wide-angle x-ray scattering (WAXS) corresponding to the lattice constant of the hexagonal packing of alkyl chain perpendicular to the L_β bilayer plane, at about 4.15 Å. [7] Self-diffusion nuclear magnetic resonance (NMR) has been adopted to evaluate the degree of swelling of the bilayers with water, that it is the key point to obtain a high volume fraction of aggregates, in which most of the water is trapped.[8]

The ternary system, surfactant/fatty alcohol/water, leads to a lamellar structure forming a percolated network giving rise to a gel. The rheological properties of the cream result from a preparation process combining high-temperature shearing and cooling steps. Indeed, the ternary system is usually heated with a temperature above the melting temperature of the fatty alcohols, homogenized and then cooled down to room temperature. The cooling step is crucial since it induces the crystallization of the long-chain alcohols and surfactants in the form of L_β bilayer, but no data are available on the link between the cooling process and the resulting rheological properties. Indeed, the present literature is mainly focused on the effect of the fatty alcohols content on the elastic modulus and the zero shear viscosity for the ternary system containing water, CTAC and fatty alcohols. [9] Recently, de Oliveira et al.

have investigated a high concentrated system made of CTAC and both cetyl and stearyl alcohols by atomistic molecular dynamics simulations, proving that the temperature used to mix the components leads to fluid bilayers, which are the units of the L_α phase. [10]

In general, a considerable number of factors, such as the nature of the continuous and dispersed phases, the phase volume ratio, particle size distributions and consequently thermal treatment influences the rheological properties of emulsions. In other words, the way on which the conditioners or other cosmetic products are prepared can affect the rheological properties. However, the effect of the thermal treatment on the structure, and, as a consequence on the rheological properties, is poorly investigated. Here, we are focusing on the effect of the cooling rate on the surfactant gel. In particular, we studied two cooling rates: fast and slow, for the very same ternary system CTAC/stearyl alcohol/water mixture. The resulting gels have markedly different rheological properties. Small angle-X-ray scattering and self-diffusion NMR were adopted to understand the microscopic reasons behind the mechanical behavior.

2. Material and Methods

2.1 Materials

All materials used were of cosmetic grade, as used for cosmetic applications. Cetearyl alcohol (50 wt.% cetyl alcohol and 50 wt.% stearyl alcohol) was purchased from BASF Cognis (Ludwigshafen, GERMANY). A commercial surfactant, cetyltrimethylammonium chloride in aqueous solution (25 wt.% in water) from BASF Cognis (Ludwigshafen, GERMANY) was used. All materials were used without further purification.

2.2 Sample preparation

All concentrations are indicated as weight percentage. The cetearyl alcohol (CA) concentration was kept constant at 5 wt.%, with 6 wt.% of cetyltrimethylammonium chloride (CTAC) in 89 wt.% of heavy water, D_2O (Sigma Aldrich) was used to facilitate ^1H diffusion NMR measurements. CA has a mass density of ca. 0.8 g/cm^3 while the density of CTAC is ca. 1.0 g/cm^3. The density of D_2O is ca. 1.1 g/cm^3. This means that the volume fraction of CTAC and CA together $\phi \approx 0.13$. Samples were prepared by first keeping samples at 85 °C in a water bath for 15 minutes under stirring. Then, two cooling processes were applied and compared. Both without stirring. In the first process after heating, the samples were rapidly

cooled down straight after preparation by putting them in a water bath with ice for one hour. Then, they were collected and stored at room temperature. In the following the samples obtained by fast cooling ,will be called quenched samples (Q). The resulting estimated cooling rate in this process was circa 40 °C/min. For the second process, the samples were allowed to cool down quiescently at room temperature without stirring, at an estimated cooling rate of 5 °C/min, hereafter called relaxed samples (R). All samples were kept at room temperature before further measurements.

2.3 Small and Wide Angle X-ray scattering

The small- and wide-angle X-ray scattering (SAXS and WAXS) profiles were obtained by radial averaging the (2D) scattering pattern recorded with the laboratory based SAXSLab Ganesha 300XL instrument (SAXSLAB ApS, Skovlunde, Denmark) using SAXSGui software. The Ganesha 300 XL is a pinhole-collimated system equipped with a Genix 3D X-ray source (Xenocs SA, Sassenage, France) and a 2D 300 k Pilatus detector (Dectris Ltd., Baden, Switzerland). Samples were sealed at room temperature in a 1.5 mm diameter quartz capillary (Hilgenberg GmbH, Mansfeld, Germany). The scattering intensity *I(q)* was recorded with the detector placed at three sample-to-detector distances of ~0.092, 0.432 and 1.482 meters, covering scattering vectors (q) in the both SAXS and WANX regions, i.e. in the range 0.004–2.8 $Å^{-1}$. In all cases, the temperature was kept constant by an external recirculating water bath fixed to 25 °C, with an accuracy of approximately 0.2 °C. The measured scattering curves were corrected for solvent scattering. In the SAXS profiles, multilamellar vesicles suspensions are characterized by various diffraction peaks, from which the repeat distance, d, of the bilayers can be calculated, $q = 2\pi n/d$, in which n is the order of the diffraction peak.

2.4 Nuclear Magnetic Resonance

^{1}H-NMR self-diffusion measurements were performed with spectrometer Agilent500 NMRS-500 equipped with OneNMR probe and have been carried out by bppste (Wu D., Chen A., Johnson C.S., J. Magn Reson (1995) 115A 260-264) with field gradient pulses ranging from 0.02 a 0.64 Tm^{-1}. The temperature of the samples was maintained at 25°C. We have used different little delta to explore several time scales and observe possible confinements for water molecules. Diffusion experiments performed with 2s of acquisition time on 16k points, gradient pulse separation, Δ, ranged from 60 ms to 2s and gradient pulse

duration, δ, ranged from 2 ms to 9 ms and Δ also represents the experimental observation time. All data were processed with the software MNova 14.1. The data were fitted according to the model developed by Krutyeva and Kärger. [11]

2.5 Rheology

The rheological measurements were carried out on an Anton Paar Physica MCR 301 instrument equipped with a cone-plate geometry (50 mm, 2°) A Peltier unit was used to control the temperature, which was fixed at 25.0 ± 0.1 °C. To minimize evaporation, an appropriate solvent trap surrounded the sample-air interface at the measuring geometry. Linear and nonlinear shear experiments were performed. The flow curves were registered from 0.01 to 100 s^{-1} for both Q and R samples, while the frequency sweep tests were performed within the linear viscoelastic regime, which was obtained by amplitude sweep tests.

3. Results and discussion

The cross-polarized microscopy pictures in Fig. 1 for both the quenched (Q) and relaxed (R) samples reveal a granular texture that is attributed to poly-dispersed and partially distorted multilamellar vesicles (MLVs) or "onion-like assemblies" since both samples were subjected to shear flow (stirring) at 85 °C where the lamellar-to-MLV transition is induced.[12] The abbreviation MLVs is adopted in the following discussion to indicate a partially distorted multilayer vesicular state. The dense state observed did not allow further analysis of the images.

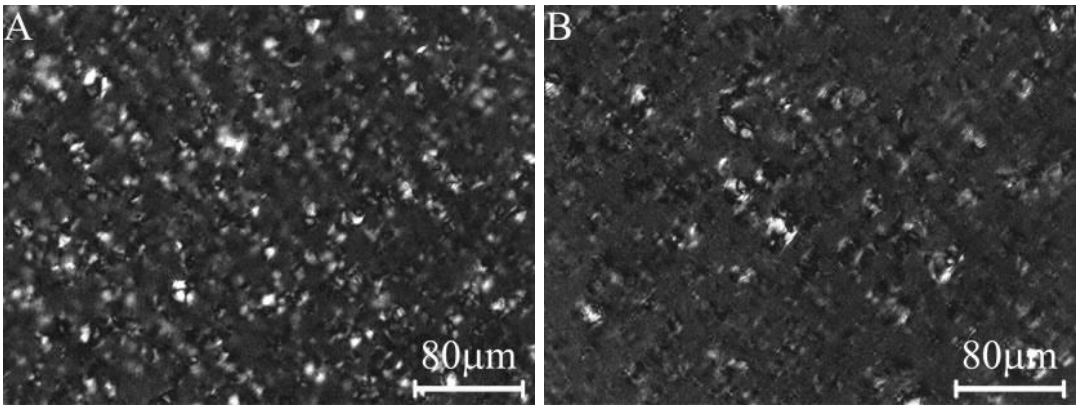

Figure 1: *Cross-polarized light microscopy images of the quenched (A) and relaxed (B) samples proving the presence of multilamellar vesicles for both samples.*

The shear-thinning behaviour of vesicles-based gels has been studied previously.[13,14] MLVs are known to exhibit shear thinning. As the shear rate is increased,

the outer shells of MLV are stripped off leading to smaller vesicles and/or lamellar sheets that do not contribute much to the viscosity of the system, or, alternatively, experience tilting in the direction of the flow with consequent alignment.[12] Both quenched (Q) and relaxed (R) samples share identical CTAC/Cetearyl alcohol composition and as such, are expected to be relatively similar on the structural point of view. However, the shear viscosity of sample Q is approximately 4 times higher than that of sample R (Figure 2). The zero shear viscosity, η_0, was out of the experimental range in the investigated systems. Figure 2 reports the shear viscosity as a function of the shear rate, $\dot{\gamma}$, and the corresponding scale, which is low for both samples Q and R. The obtained scaling law of $\eta \propto \dot{\gamma}^{-0.74}$ and $\eta \propto \dot{\gamma}^{-0.69}$ for Q and R, respectively, matches previous observation on the shear thinning of MLVs. A scaling factor between 0.55 and 0.8 has been found for several systems depending on the surfactant concentration[15–18], while higher values were detected in the presence of planar lamellae [18].

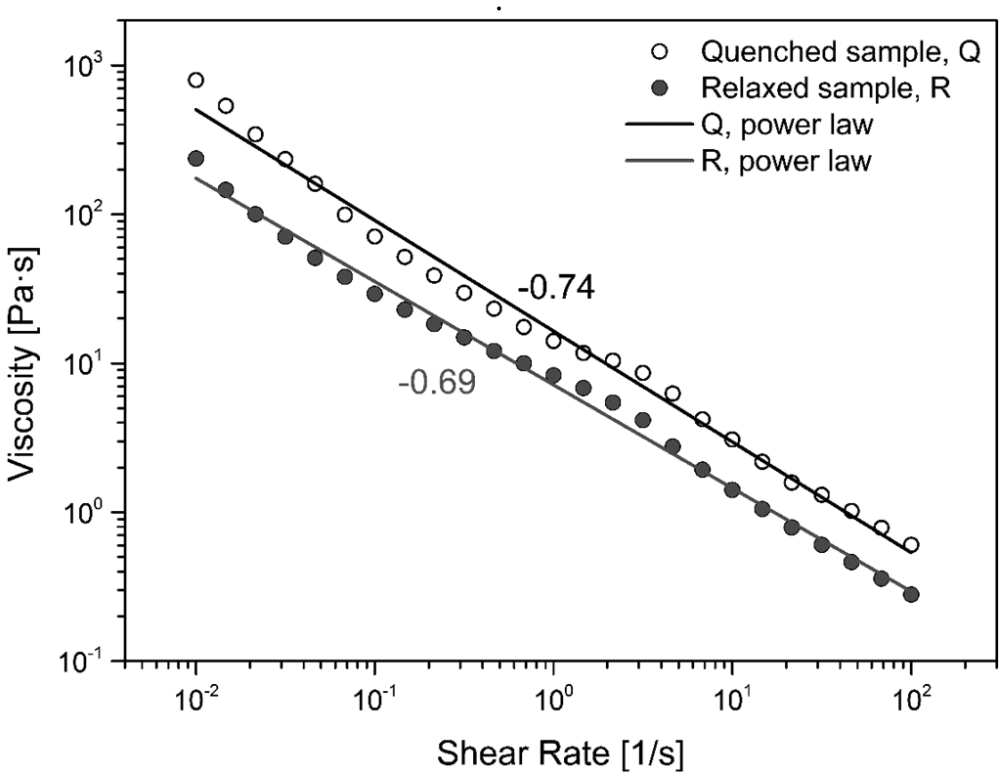

Figure 2: *Flow curve of the quenched (Q) and relaxed (R) samples in the shear rate range between 0.01 and 100 s^{-1} measured at 25 °C.*

The diffusional properties of water (strictly HDO) in both systems was probed by collecting the PGSE-NMR echo decays that are shown in Fig. 3 as a function of the

experimental variable b^2t where b = (γgδ) and t = (Δ-δ/3) obtained by varying the gradient strength (g) while keeping the gradient pulse length (δ) and the gradient pulse separation (Δ) constant within each experimental run; γ is the gyromagnetic ratio of the observed nucleus (^{1}H). Such technique has been widely applied to study molecular diffusion in micro-compartmentalized systems and was discussed in detail in reviews [19–21] and textbooks. [22] The outcome of PGSE-NMR experiments in systems where the spin bearing molecule is secluded by some barriers (e.g. lamellae, emulsion droplets, capillaries and so on) that hinder its translational degrees of freedom depends on the ratio between the experimental time scale (dictated by Δ) and residence time of the molecule in a given site τ [23]. In the case of fast exchange, the echo decays exponentially as a function of b^2t and is characterized by a single *apparent* diffusion coefficient that is the population average of the diffusion coefficients in the different sites. On the other hand, when the molecular exchange is slow compared to the experimental timescale (τ<<Δ) the echo attenuation becomes multi-exponential, reflecting the different diffusion coefficient probed by the spins.

In the intermediate case of τ ~Δ the situation is more complicated, and the shape of the decay could deviate from the simple sum of exponentials. The echo decays of Fig. 3 are, for both samples, clearly bimodal with an almost exponential fast phase and a non-exponential slow phase. Considering the present system is made of a large volume fraction of MLVs with a smaller amount of water in between, we have fitted the data using a two-site discrete exchange model in the intermediate exchange time regime. The echo attenuation is represented in terms of water diffusion in the inter-vesicle space (fast diffusing with a diffusion coefficient D_F) and within MLVs (slow diffusing with a diffusion coefficient D_S) and of their relative populations P_F and P_S= (1- P_F). Assuming fast diffusing inter-vesicular water is only a small fraction (P_F << P_S and D_F >> D_S) the echo attenuation (E(q,t)) becomes:[11]

$$E(b,t) = exp\left(-b^2\left(D_s + \frac{p_F D_F}{b^2\tau_s p_F D_F + 1}\right)t\right) \qquad eq.1$$

where the molecular mean residence time in the MLVs (slow diffusion state) is denoted by τ_s.

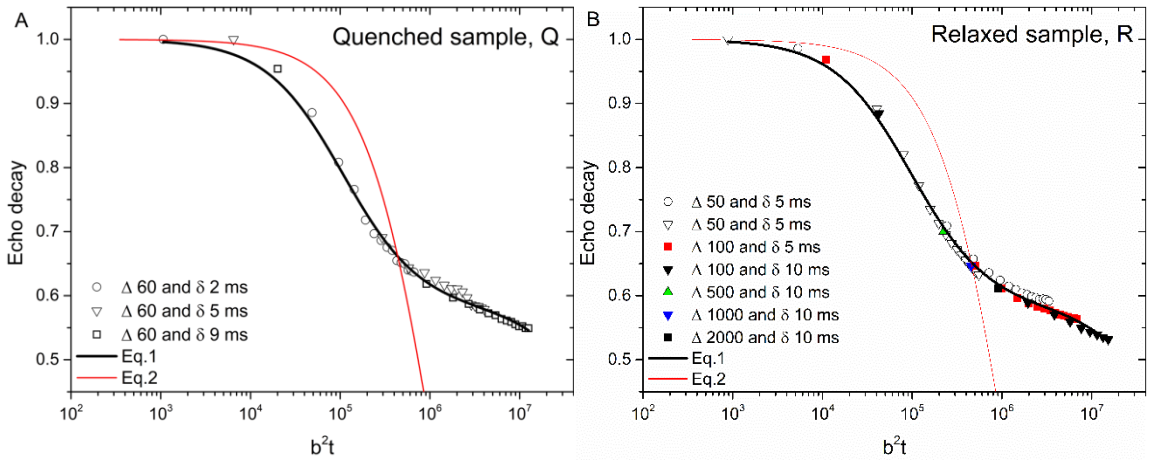

Figure 3: Experimental echo decays (symbols) and best fit of Eq. 1 to the data (solid line) for: (A) the quenched sample, Q and (B) the relaxed sample, R. The red solid line is the planar lamellae echo decay model to appreciate differences (Eq.2).

Best fits of Eq. 1 to the experimental echo decays are shown in Figure 3 as solid lines. The three independent fitting parameters were D_s, P_fD_f and τ_s. Parameter values are presented in Table 1.

It should be emphasized that the well-known echo-decay for planar lamellar phase [24] described by equation 2 below (where x is an integration variable) does not account for the experimental echo-decay, as reported in Figure 3.

$$I(b,t) = e^{-q^2Dt}\int_0^1 e^{x^2b^2Dt}dx \qquad (2)$$

Table 1. Parameters obtained from fitting Eq. (1) to the echo attenuation data of Fig. 3.

	p_fD_f / m^2s^{-1}	D_s / m^2s^{-1}	τ_s /s
Quenched Sample	$(3.9 \pm 0.1)10^{-10}$	$(5.4 \pm 0.8)10^{-13}$	0.110 ±0.0001
Relaxed Sample	$(4.2 \pm 0.1)10^{-10}$	$(6.6 \pm 0.7)10^{-13}$	0.0921±0.0007

The best-fit data listed in Table 1 can be combined to gain insight on some aspects of the microstructure of the system. The two-sites model at the basis of equation 1 foretells a relation between the radius (R) of the slow diffusing domain and the residence time according to $\frac{R^2}{15\,D_s} = \tau_s$.[25] Using the values of Table 1 one obtains sizes (2R) of the order of 2 μm, which isreasonable for giant MLVs.

The term $p_f D_f$ allows an estimate of the fraction of water secluded in the MLV. Assuming the water outside the MLV diffuses as neat D_2O ($18x10^{-10}$ m^2s^{-1}) we have that the mole fraction of water within the MLV ($1-p_f$) is around 78 mol% corresponding to a 69% in volume. To estimate the MLV overall volume fraction (that matter for rheological response) one has to add to this value the 13% of the organic phase obtaining as an estimate for the volume fractions occupied by the MLV ϕ_{MLV} =0.81 which points to samples in which almost all the available volume is occupied by lamellar vesicles. However the difference between the ϕ_{MLV} for the two systems is only around 2%, thus not enough to explain the factor 4 on the viscosity values [26].

To investigate structural differences between the two vesicular systems, small and wide-angle X-ray scattering (SAXS/WAXS) experiments were performed at 25 °C on both samples. The data are presented in Fig. 4. The scattering profiles of quenched and relaxed samples are very similar and are consistent with MLVs and a locally lamellar structure. A q^{-2} decay is observed at lower q-values with a first-order quasi-Bragg peak at $q = q_{Q1} \approx 0.02$ $Å^{-1}$ and $q = q_{R1} \approx 0.022$ $Å^{-1}$, confirming the lamellar order with an average periodicity of $d_Q = 2\pi/q_{Q1} \approx 31.4$ nm, $d_R = 2\pi/q_{R1} \approx 28.5$ nm. The peaks are, however, weak and can be seen more clearly and evaluated more accurately in a so-called Kratky plot, $I(q)q^2$ versus q, shown as an inset in Fig. 4. From the Kratky plot, a weak second-order peak at $q \approx 0.04$ $Å^{-1}$ can be appreciated clearly for the quenched sample. The fact that the quasi-Bragg peaks are weak implies that there is a broad polydispersity in the *d*-spacing.

The theoretical maximum interlamellar *d*-spacing for an L_β phase can be calculated using eq. 3 [7]

$$d_{max} = \frac{10^{24}\sqrt{3}}{a^2 C_T N_{av}} \qquad eq.3$$

where C_T is the total acyl chain concentration in mol/l, N_{av} is the Avogadro constant and *a* is the inter-acyl lattice constant, obtained from the sharp WAXS peak, equal to 0.455 nm ($2\pi/q_{peak}$), in literature a value around 0.42 nm is often reported [7]. The resulting d_{max} is 31.2 nm, implying that the L_β phase-swell is around 100% for the (fast-cooling) Q-sample, while it is around 90% for the (slow-cooling) R-sample. The relaxed sample seems to be better described by a lamellar gel network that is a multi-phase composed mainly of L_β phase, while the quenched sample is ascribed by a pure L_β phase.

At $q \approx 0.1$ $Å^{-1}$ there is a cross-over from a q^{-2} to a q^{-4} decay and, in addition, a broad intensity maximum at $q \approx 0.4$ $Å^{-1}$. This q-range describes the bilayer cross-section form

factor, $P_{cs}(q)$, from which we can evaluate a bilayer thickness, δ. The contrast in X-ray scattering comes from differences in electron density. [27] The scattering length density (proportional to the electron density) profile of charged surfactant/lipid bilayers in the normal direction is often characterized by maxima in the polar head group regions, and a minimum in the center. Here we modelled the scattering length density profile $\Delta\rho(z) = \rho(z)-\rho_w$, as a sum of three rectangular boxes using the SasView software.[28] ρ(z) describes the variation in electron density in the z-direction, perpendicular to the bilayer, and $\rho_w = 9.5\ 10^{-6}$ Å^{-2} is the water (solvent) scattering length density. Δρ(z) refers to the excess (with respect to solvent) electron density. In the hydrocarbon region of the bilayer we expect $\rho = 7.8\ 10^{-6}$ Å^{-2}. As an insert in Fig. 4, we highlight the scattering profiles in the *q*-range 0.1-0.5 Å^{-1}, including a calculated scattering profile. In the calculations we assumed a bilayer model composed of a 3.0 nm thick hydrocarbon region sandwiched between two 0.4 nm thick head-group regions having a higher, $\rho = 12\ 10^{-6}$ Å^{-2}, scattering length density. This corresponds to a total bilayer thickness of $\delta = 3.8$ nm, similar to what was obtained in a simulation of a similar bilayer composition.[10]

With the values of $\delta \approx 3.8$ nm, $d_Q \approx 31.4$ nm and $d_R \approx 28.5$ nm we are able to estimate a volume fraction, ϕ_{in}, of CTAC+CA *inside* the MLVs, since $\phi_{Q,in} = \delta/d_Q \approx 0.12$ and $\phi_{R,in} = \delta/d_R \approx 0.13$. The MLVs volume fraction is obtained by the ratio $\phi_{Q,MLV} = \phi/\phi_{Q,in} \approx 0.83$ and $\phi_{R,MLV} = \phi/\phi_{R,in} \approx 0.77$, where ϕ the overall volume fraction of CTAC+CA is ~0.1 (considering all CTAC and CA are present in the MLV bilayers). These values are very close to the volume fraction of MLVs evaluated by PGSE-NMR (ϕ_{MLV}*~0.81*).This indicates that almost all the L_β bilayers are in the form of (distorted) multilamellar vesicles.

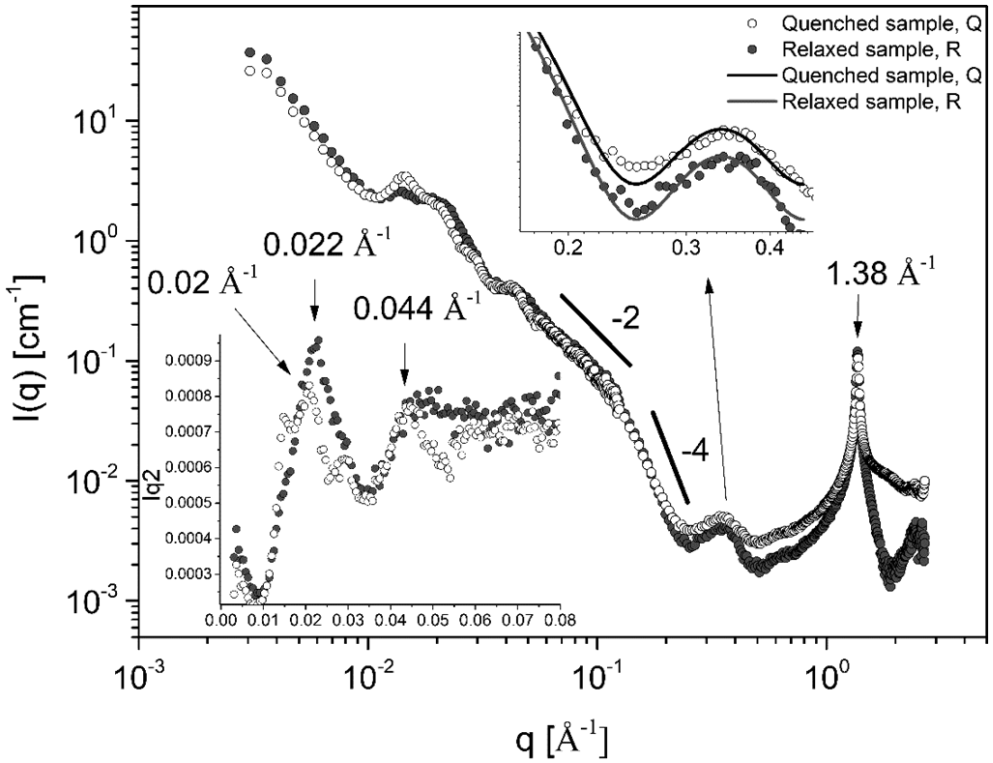

Figure 4: Small-angle X-ray scattering (SAXS) profiles of samples Q and R obtained by averaging all directions of radially symmetrical 2D patterns. The inset at low-q is the Kratky plot of the same data, while the inset in the q-range between 0.2 and 0.4 $Å^{-1}$ reports the fitted data using the Nallet model [29]. The fitting parameters were the following ρ_{head} = 12e-06 $Å^{-2}$; ρ_w = 9.47e-06 $Å^{-2}$; ρ_{tail} = 7.81e-06 $Å^{-2}$; tail length = 15 Å and head thickness = 4 Å. In the Nallet model, the total thickness of the bilayer is given by 2(tail length+ head thickness) = 3.8 nm.

The frequency sweep demonstrated a similar behavior of the two samples along the investigated frequency region. However, G′ and G″ are considerably higher for the quenched sample Q respect to the relaxed sample R, confirming the flow curve results. The amplitude sweep in Figure 5 shows the absence of a yield point as expected for a vesicle-based gel [30].

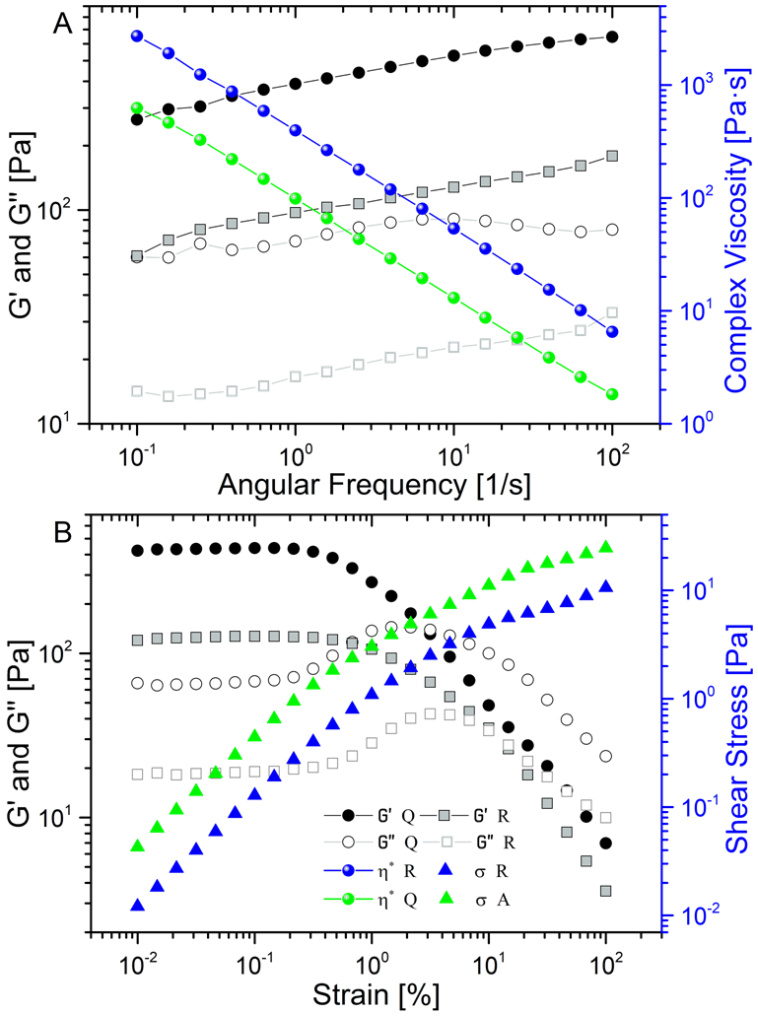

Figure 5: Frequency (A) and amplitude (B) sweep measurements on the quenched, Q, and relaxed, R, samples. The frequency sweep is performed in the linear viscoelastic regime. The frequency sweep was performed in the linear viscoelastic regime at strain 0.1%.

For the MLVs phase, the G″ value is less than 1 order of magnitude smaller than G′. Such a difference has been reported for several MLVs phases [18]. The main contribution to the elastic modulus G′ could come from the affine motion on the length scale of the MLVs size or the *d*-spacing scale. The affine motion on the length scale of the *d*-spacing has been demonstrated to have a considerable effect [31]. Combining the equation proposed by Versluis et al. [32] with the relationship between the compression modulus and *d*-spacing in the case of more rigid bilayers (i.e. L_β) [33], the average bilayer bending rigidity, K, can be estimated

$$K = \frac{4}{n}\frac{G'}{tan^2\theta}d^3 \qquad eq.4$$

Where 2θ is the top angle of the cone over which two adjacent MLVs interact, i.e. $tan^2\theta = 0.2$, d is the *d*-spacing and n the number of neighbours (= 10), while G′ is the

value at 0.1 rad/s and 0.1 % strain. The bending rigidities obtained are equal to ~6.3 and ~1.4 k_bT, demonstrating a change in the bilayer composition, i.e. a different CTAC/stearyl alcohol ratio in the MLVs. The reported values are in agreement with the literature since for charged lamellae higher bending rigidity is expected ~ 50 kbT [34] but fatty alcohols are lowering down by an order of magnitude such a value [35].

The large mechanical differences between the two concentrated gel systems made of CTAC/Cetearyl alcohol in water, by fast- (quenched sample) and slow- (relaxed sample) cooling is mainly due to the nature of the phase state of the bilayers and their average bilayer bending rigidity. Moreover the total MLV volume fraction is slightly higher for sample Q. In fact, the quenched sample is essentially pure L_β state that is characterized by a high rigidity of the bilayer, while the relaxed sample is a mixture of phases and the average bending rigidity is therefore affected. In both cases, the L_β phase is mainly present in the form of MLVs.

Due to the high rigidity, it is not common to obtain a full swell of the L_β phase, however, in the present preparation the presence of the fatty alcohol and high temperature during preparation allowed the full swell and MLVs formation. The fast cooling quenches such a situation leading to fully swollen MLVs, subsequently "frozen" by the quenching process. On the other hand, during the slow-cooling process, the system has the time to relax to its equilibrium condition dictated by the bending rigidity consequently the full swell of the L_β phase is not favorable and the formation of other bilayer phase states is allowed.

Table 2 reports the main findings discussed.

Table 2. Experimental results and calculated parameters of the fast and slow- cooling samples. [a]from SAXS; [b]from rheology at frequency 0.1 rad/s and Strain 0.1%; [c]calculated from rheology and SAXS data.

	Quenched sample, Q (fast-cooling)	**Relaxed sample, R (slow-cooling)**
Volume fraction (%)[a]	~0.83	~0.77
Elastic modulus G' (Pa)[b]	420±20	120±10
d-spacing (nm)[a]	31.4±0.5	28.5±0.5
Bilayer thickness (nm)[a]	3.8±0.2	
Bending rigidity (k_bT)[c]	~6.3	~1.4
Lamellar phase	L_β	*~90% of* L_β

4. Conclusions

The effect of the cooling process on the surfactant gel made of CTAC/Cetearyl alcohol in water was investigated in detail for the first time. In particular, the cooling rate effect on the structure was examined by SAXS, diffusion-NMR and rheology.

SAXS data demonstrated that the *d*-spacing between the bilayers was 31.4 nm for the fast-cooling sample and 28.5 nm for the slow-cooling sample, while the bilayer thickness was ~3.8 nm for both, implying a lower volume fraction for the fast cooling sample. Moreover, the fast-cooling sample is essentially in the L_β phase, while the slow-cooling sample shows ~90% in the L_β state, i.e, a lamellar gel network can describe it. Moreover, the average bilayer bending rigidity was calculated considering the elastic modulus and the *d*-spacing of the respective samples. The quenched (fast-cooling) sample has a bilayer bending rigidity almost 5 times higher than the relaxed (slow-cooling) sample because the latter is made by multiple-phases. We conclude the cooling speed is affecting the phase state of CTAC/stearyl alcohol bilayers.

Here we have provided a structural explanation to the large mechanical differences in the rheological properties induced by only changing the cooling rate while keeping constant the chemical composition.

Acknowledgements

This project has received funding from the European Union's Horizon 2020 research and innovation programme under grant agreement No 731019 (EUSMI). G.C., G.P., H.M. and L.G., are thankful to the Center for Colloid and Surface Science (CSGI) for the financial support.

References

[1] L. Rhein, Surfactant Action on Skin and Hair. Cleansing and Skin Reactivity Mechanisms, in: Handbook for Cleaning/Decontamination of Surfaces, Elsevier, 2007: pp. 305–369. https://doi.org/10.1016/B978-044451664-0/50009-7.

[2] M.M. Rieger, L.D. Rhein, eds., Surfactants in cosmetics, 1997.

[3] T.S. Awad, E.S. Johnson, A. Bureiko, U. Olsson, Colloidal structure and physical properties of gel networks containing anionic surfactant and fatty alcohol mixture, Journal of Dispersion Science and Technology. 32 (2011) 807–815. https://doi.org/10.1080/01932691.2010.488134.

[4] G.M. Eccleston, Functions of mixed emulsifiers and emulsifying waxes in dermatological lotions and creams, Colloids and Surfaces A: Physicochemical and Engineering Aspects. 123–124 (1997) 169–182. https://doi.org/10.1016/S0927-7757(96)03846-0.

[5] D. Balzer, S. Varwig, M. Weihrauch, Viscoelasticity of personal care products, Colloids and Surfaces A: Physicochemical and Engineering Aspects. 99 (1995) 233–246. https://doi.org/10.1016/0927-7757(95)03144-3.

[6] H.E. Junginger, Colloidal structures of O/W creams, Pharmaceutisch Weekblad Scientific Edition. 6 (1984) 141–149. https://doi.org/10.1007/BF01954041.

[7] T. Iwata, Lamellar gel network, in: Cosmetic Science and Technology: Theoretical Principles and Applications, Elsevier Inc., 2017: pp. 415–447. https://doi.org/10.1016/B978-0-12-802005-0.00025-2.

[8] F. Grewe, J. Ortmeyer, R. Haase, C. Schmidt, Colloidal gels formed by dilute aqueous dispersions of surfactant and fatty alcohol, in: Colloid Process Engineering, Springer International Publishing, 2015: pp. 20–44. https://doi.org/10.1007/978-3-319-15129-8_2.

[9] J. Nakarapanich, T. Barameesangpet, S. Suksamranchit, A. Sirivat, A.M. Jamieson, Rheological properties and structures of cationic surfactants and fatty alcohol emulsions: Effect of surfactant chain length and concentration, Colloid and Polymer Science. 279 (2001) 671–677. https://doi.org/10.1007/s003960000470.

[10] T.E. de Oliveira, F. Leonforte, L. Nicolas-Morgantini, A.-L. Fameau, B. Querleux, F. Thalmann, C.M. Marques, Fluid bilayer phase in aqueous mixtures of fatty alcohol and cationic surfactant, Physical Review Research. 2 (2020). https://doi.org/10.1103/physrevresearch.2.013075.

[11] M. Krutyeva, J. Kärger, NMR Diffusometry with Beds of Nanoporous Host Particles: An Assessment of Mass Transfer in Compartmented Two-Phase Systems, Langmuir.

24 (2008) 10474–10479. https://doi.org/10.1021/la801426f.

[12] L. Gentile, M.A. Behrens, L. Porcar, P. Butler, N.J. Wagner, U. Olsson, Multilamellar vesicle formation from a planar lamellar phase under shear flow, Langmuir. 30 (2014) 8316–8325. https://doi.org/10.1021/la501071s.

[13] M. Gradzielski, The rheology of vesicle and disk systems - Relations between macroscopic behaviour and microstructure, Current Opinion in Colloid and Interface Science. 16 (2011) 13–17. https://doi.org/10.1016/j.cocis.2010.07.005.

[14] R. Angelico, M. Carboni, S. Lampis, J. Schmidt, Y. Talmon, M. Monduzzi, S. Murgia, Physicochemical and rheological properties of a novel monoolein-based vesicle gel, Soft Matter. 9 (2013) 921–928. https://doi.org/10.1039/c2sm27215f.

[15] J. Bergenholtz, N.J. Wagner, Formation of AOT/Brine Multilamellar Vesicles, Langmuir. 12 (1996) 3122–3126. https://doi.org/10.1021/la950696n.

[16] D. Roux, F. Nallet, O. Diat, Rheology of lyotropic lamellar phases, EPL. 24 (1993) 53–58. https://doi.org/10.1209/0295-5075/24/1/009.

[17] E. van der Linden, W.T. Hogervorst, H.N.W. Lekkerkerker, Relation between the Size of Lamellar Droplets in Onion Phases and Their Effective Surface Tension, Langmuir. 12 (1996) 3127–3130. https://doi.org/10.1021/la950950b.

[18] L. Gentile, B.F.B. Silva, S. Balog, K. Mortensen, U. Olsson, Structural transitions induced by shear flow and temperature variation in a nonionic surfactant/water system, Journal of Colloid and Interface Science. 372 (2012) 32–39. https://doi.org/10.1016/j.jcis.2012.01.027.

[19] P. Stilbs, Fourier transform pulsed-gradient spin-echo studies of molecular diffusion, Progress in Nuclear Magnetic Resonance Spectroscopy. 19 (1987) 1–45. https://doi.org/10.1016/0079-6565(87)80007-9.

[20] B. Lindman, U. Olsson, Structure of Microemulsions Studied by NMR, Berichte Der Bunsengesellschaft Für Physikalische Chemie. 100 (1996) 344–363. https://doi.org/10.1002/bbpc.19961000321.

[21] J. KÄRGER, H. Pfeifer, W. Heink, Principles and Application of Self-Diffusion Measurements by Nuclear Magnetic Resonance, in: Advances in Magnetic and Optical Resonance, 1988: pp. 1–89. https://doi.org/10.1016/B978-0-12-025512-2.50004-X.

[22] P.T. Callaghan, Principles of nuclear magnetic resonance imaging, 1993.

[23] I. Slund, B. Medronho, D. Topgaard, O. Söderman, C. Schmidt, Homogeneous length scale of shear-induced multilamellar vesicles studied by diffusion NMR, Journal of Magnetic Resonance. 209 (2011) 291–299. https://doi.org/10.1016/j.jmr.2011.01.024.

[24] P.T. Callaghan, K.W. Jolley, J. Lelievre, Diffusion of water in the endosperm tissue of wheat grains as studied by pulsed field gradient nuclear magnetic resonance, Biophysical Journal. 28 (1979) 133–141. https://doi.org/10.1016/S0006-3495(79)85164-4.

[25] J. Kärger, R. Valiullin, Mass transfer in mesoporous materials: The benefit of microscopic diffusion measurement, Chemical Society Reviews. 42 (2013) 4172–4197. https://doi.org/10.1039/c3cs35326e.

[26] I.M. Krieger, T.J. Dougherty, A Mechanism for Non- Newtonian Flow in Suspensions of Rigid Spheres, Transactions of the Society of Rheology. 3 (1959) 137–152. https://doi.org/10.1122/1.548848.

[27] P. (Peter) Lindner, T. (Thomas) Zemb, Neutron, X-rays and Light. Scattering Methods Applied to Soft Condensed Matter, Elsevier, 2005. https://doi.org/10.1016/s1369-7021(02)01143-4.

[28] SasView - Small Angle Scattering Analysis, (n.d.). https://www.sasview.org/ (accessed February 13, 2020).

[29] F. Nallet, R. Laversanne, D. Roux, Modelling X-ray or neutron scattering spectra of lyotropic lamellar phases : interplay between form and structure factors, Journal de Physique II. 3 (1993) 487–502. https://doi.org/10.1051/jp2:1993146.

[30] E. Brown, H. Zhang, N.A. Forman, B.W. Maynor, D.E. Betts, J.M. Desimone, H.M. Jaeger, Shear thickening and jamming in densely packed suspensions of different particle shapes, Physical Review E - Statistical, Nonlinear, and Soft Matter Physics. 84 (2011). https://doi.org/10.1103/PhysRevE.84.031408.

[31] P. Panizza, † D Roux, V. Vuillaume, C.-Y.D. Lu, M.E. Cates, Articles Viscoelasticity of the Onion Phase, 1996. https://pubs.acs.org/sharingguidelines (accessed January 31, 2020).

[32] P. Versluis, J.C. Van De Pas, J. Mellema, Influence of Salt Concentration and

Surfactant Concentration on the Microstructure and Rheology of Lamellar Liquid Crystalline Phases, (2001). https://doi.org/10.1021/la000779q.

[33] D. Boal, Mechanics of the cell, second edition, 2012. https://doi.org/10.1017/CBO9781139022217.

[34] H.A. Faizi, S.L. Frey, J. Steinkühler, R. Dimova, P.M. Vlahovska, Bending rigidity of charged lipid bilayer membranes, Soft Matter. 15 (2019) 6006–6013. https://doi.org/10.1039/c9sm00772e.

[35] S. Hebbar, E. Knust, G. Thibault, R.S. Kraut, Editorial: Connections to Membrane Trafficking Where You Least Expect Them: Diseases, Dynamics, Diet and Distance, Frontiers in Cell and Developmental Biology. 7 (2019). https://doi.org/10.3389/fcell.2019.00327.